Supplementary Information

Photo-accelerated Co^{3+}/Co^{2+} Transformation on Cobalt and Phosphorus Co-doped g-C_3N_4 for Fenton-like Reaction

Xiaomei Liu,[a] Yang Li,[ab] Xiaobin Fan,[ab] Fengbao Zhang,[a] Guoliang Zhang [a] and Wenchao Peng *[ab]

[a] School of Chemical Engineering and Technology, Tianjin University, Tianjin, 300350, China.
[b] Chemistry and Chemical Engineering Guangdong Laboratory, Shantou, 515031, China

*Corresponding author: Wenchao Peng, E-mail: wenchao.peng@tju.edu.cn

Text S1. Materials and Reagents

Urea (CH_4N_2O, 99%), hexachlorotriphosphazene (HCCP, 98%), cobalt (II) acetate tetrahydrate ($Co(CH_3COO)_2{\cdot}4H_2O$, >99.5%), potassium persulfate ($K_2S_2O_8$, 99.99%), bisphenol A (BPA, GR), 1, 4-benzoquinone (BQ, 99.5%), potassium chloride (KCl, 99.5%) and potassium nitrate (KNO_3, 99%) were obtained from Aladdin Chemistry Co., Ltd., Shanghai, China. Tertbutyl alcohol (TBA, HPLC), ethanol (≧99.7%) and methyl alcohol (MeOH, HPLC) were purchased from Tianjin Kermel Chemical Reagent Co., Ltd. Furfuryl alcohol (FFA, 99%), potassium dichromate ($K_2Cr_2O_7$, 99.8%), disodium ethylenediaminetetraacetate dihydrate (EDTA-2Na, 99%), triethanolamine (TEOA, 98%) and sodium sulphate (Na_2SO_4, 99%) were provided by Tianjin Guangfu Fine Chemical Research Institute. Potassium bicarbonate ($KHCO_3$, 99.5%) and potassium dihydrogen phosphate (KH_2PO_4, 99.5%) were purchased from Macklin Reagent (Shanghai, China). Hydrochloric acid (HCl, 36%-38%) and sodium hydroxide (NaOH, 97%) were obtained from Tianjin Damao Chemical Reagent Co., Ltd. All the chemicals and reagents were used as received without further purification. The deionized water was used in all experiments.

Text S2. Characterization

The phase composition was characterized by X-ray diffraction (XRD, BrukerNonius D8 Focus diffractometer). The morphologies of samples were recorded by scanning electron microscopy (SEM, Hitachi, Regulus 8100) and transmission electron microscopy (TEM, JEM-2100F). X-ray photoelectron spectroscopy (XPS) and XPS valence band (VB-XPS) were analyzed by a PerkinElmer PHI1600 spectrometer. Fourier transform infrared spectroscopy (FT-IR, Thermo-Nicolet 380) was applied to characterize the structure of samples. N_2 adsorption and desorption isotherms and pore size distribution were measured on a Bjbuilder SSA-7000. UV-vis diffused reflectance spectra (UV-vis DRS) were obtained by a UV-vis spectrophotometer (PerkinElmer Lambda 35) equipped with an integrating sphere using $BaSO_4$ as the reference. The photoluminescence (PL) emission spectra were determined on a fluorophotometer (Edinburgh FLS1000, excited at 350 nm). The photoelectrochemical properties were measured on a standard three-electrode electrochemical analyzer of Shanghai Chenhua CHI660E. An Ag/AgCl electrode, Pt plate, and fluorine-doped SnO_2 (FTO, 2.0 cm×1.0 cm) glass electrode coated with catalyst with a cover area of 1.0 cm^2 were used as the reference electrode, counter electrode and working electrode, respectively. 0.5 M Na_2SO_4 aqueous solution (pH ≈ 7.0) was employed as the electrolyte. Electrochemical impedance spectroscopy (EIS) was conducted with the frequency range from 0.1 Hz-1000 kHz under open circuit potential. The transient photocurrent response was evaluated under pulsed light irradiation (light on or off cycles: 30 s). The Mott-Schottky plots were obtained at an amplitude of 5 mV and varied frequencies of 500, 750, and 1000 HZ, respectively. The conversion from the measured potential vs. Ag/AgCl to the potential vs. normal hydrogen electrode (NHE) follows Nernst equation:

$$E\,(NHE) = E\,(Ag/AgCl) + 0.0592\times pH + 0.197. \quad (S1)$$

Text S3. Operation parameters

To better understand the characteristic of BPA degradation by Co, P-CN activated PDS under light irradiation, the rational operation parameters on BPA degradation are explored, including catalyst dosage and PDS concentration. Fig. S9a displays the influence of catalyst dosage on BPA degradation. The efficiency of BPA degradation is increased with increasing the dosage of catalyst from 0 to 0.8 g/L. When the catalyst dosage is 0.6 and 0.8 g/L, BPA can be eliminated completely within 15 min. From the perspective of economic cost, 0.6 g/L is selected as the optimal catalyst dosage. What's more, excessive catalyst will hinder the light transmission and penetration into the bulk solution, resulting in poor light utilization.[1] Fig. S9b shows BPA degradation efficiency at various PDS concentration. The BPA removal efficiency is first increased along with the increasing PDS concentration from 0 g/L to 2.0 g/L, and then is decreased slightly from 2.0 g/L to 4.0 g/L, confirming that the optimal PDS concentration is 2.0 g/L. The excessive PDS concentration leads to decreased removal efficiency of BPA, which might be attributed to the self-quenching effect from the excessive radicals.[2]

Text S4. Density functional theory (DFT) calculations

The models were computed with density functional theory (DFT) using projected augment wave method as implemented in the Vienna ab initio Simulation Package (VASP) code.[3,4] The generalized gradient approximation (GGA) of Perdew-Burke-Ernzerhof (PBE) is used for the exchange-correlation potential.[5] Plane-wave basis set was used with an energy cutoff of 600 eV. The convergence criterion for electronic structure iteration was set to be 1×10^{-5} eV and structural optimization would be terminated until all forces were smaller than 0.05 eV/Å. Polarization effect was considered and the van der Waals (vdW) interactions were taken into consideration by using the method of Grimme (DFT-D3). The charge transfer was analyzed by calculating the charge density using the Bader charge analysis method.[6] A 15 Å vacuum space was introduced to avoid interactions between adjacent layers, k-mesh was set as 3×3×1 in this work. The adsorption energy was defined as:

$$E_{ads} = E_{cluster + PDS} - E_{cluster} - E_{PDS} \quad \text{(S2)}$$

Where $E_{cluster + PDS}$, $E_{cluster}$ and E_{PDS} represent for the total energy of the model, the energy of the cluster model and the energy of free PDS, respectively.

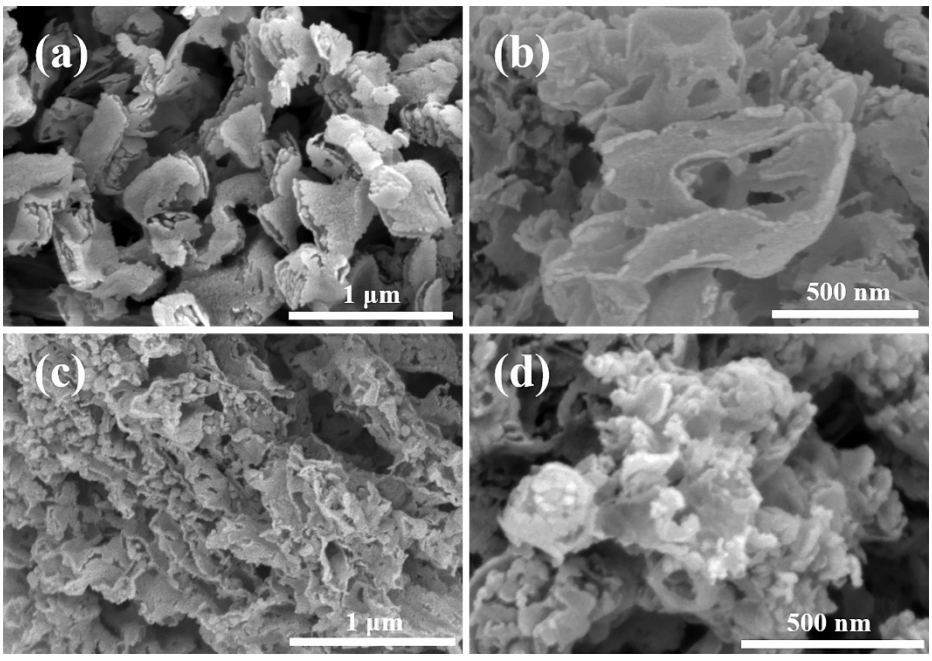

Fig. S1 SEM images of (a) CN, (b) P-CN, (c) Co-CN, and (d) Co, P-CN samples.

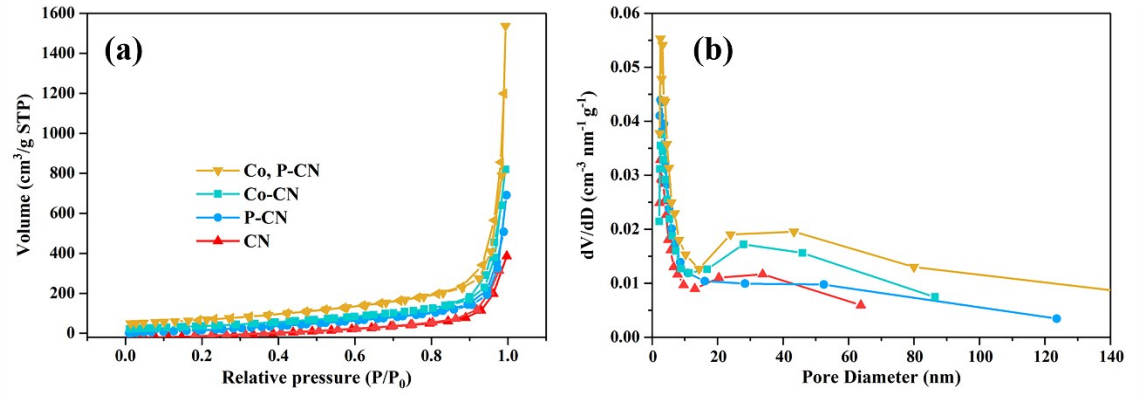

Fig. S2 N_2 adsorption-desorption isotherms (a) and pore size distributions (b) of as-prepared CN, P-CN, Co-CN, and Co, P-CN samples.

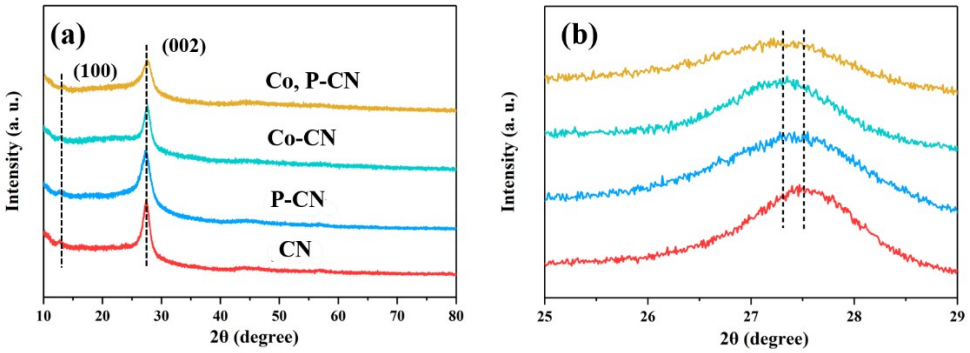

Fig. S3 (a) XRD patterns and (b) the enlarged view of characteristic peak at 27.5° of the prepared CN, P-CN, Co-CN, and Co, P-CN samples.

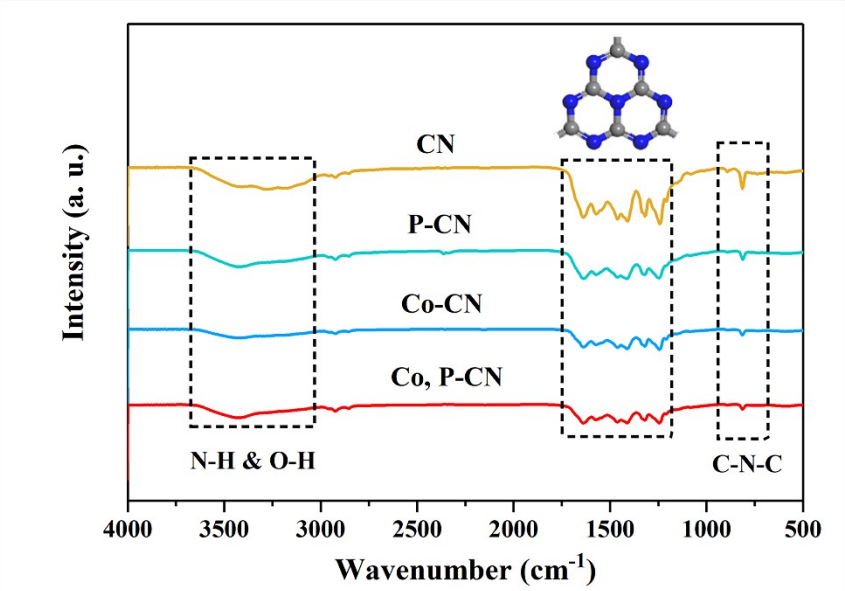

Fig. S4 FT-IR spectra of the prepared CN, Co-CN, P-CN and Co, P-CN samples.

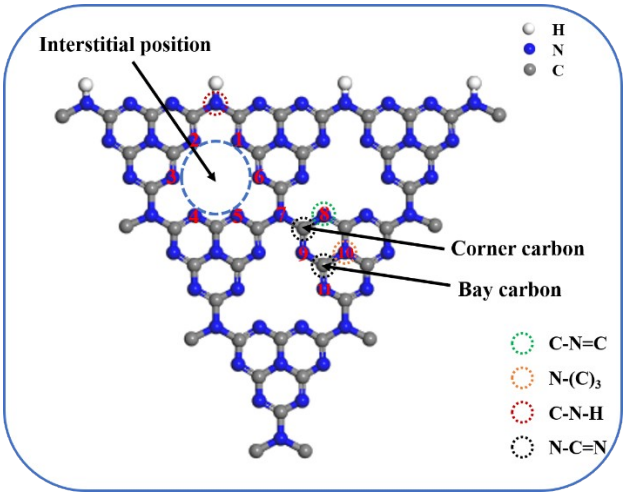

Fig. S5 The bonding schematic diagram of g-C_3N_4 and the doping sites of Co and P in g-C_3N_4 structure.

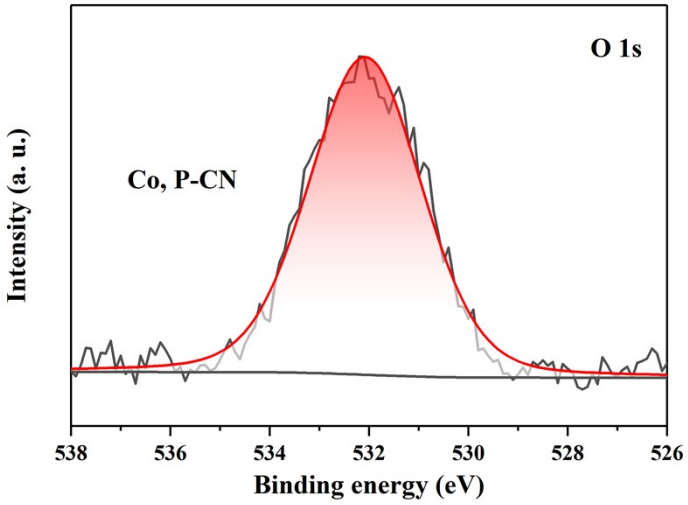

Fig. S6 High-resolution O 1s XPS spectrum of Co, P-CN sample.

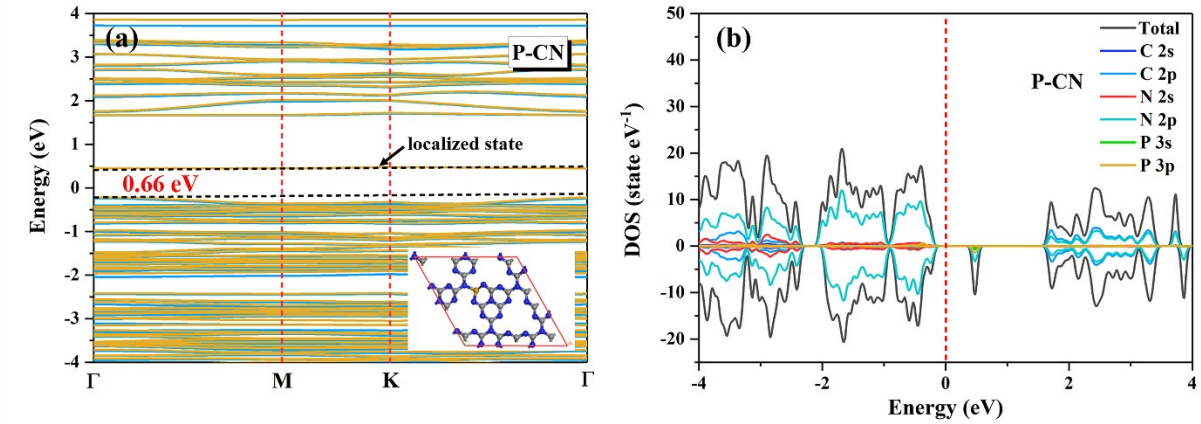

Fig. S7 Band structure (a), optimized structure (the inset of a) and DOS (b) of P-CN.

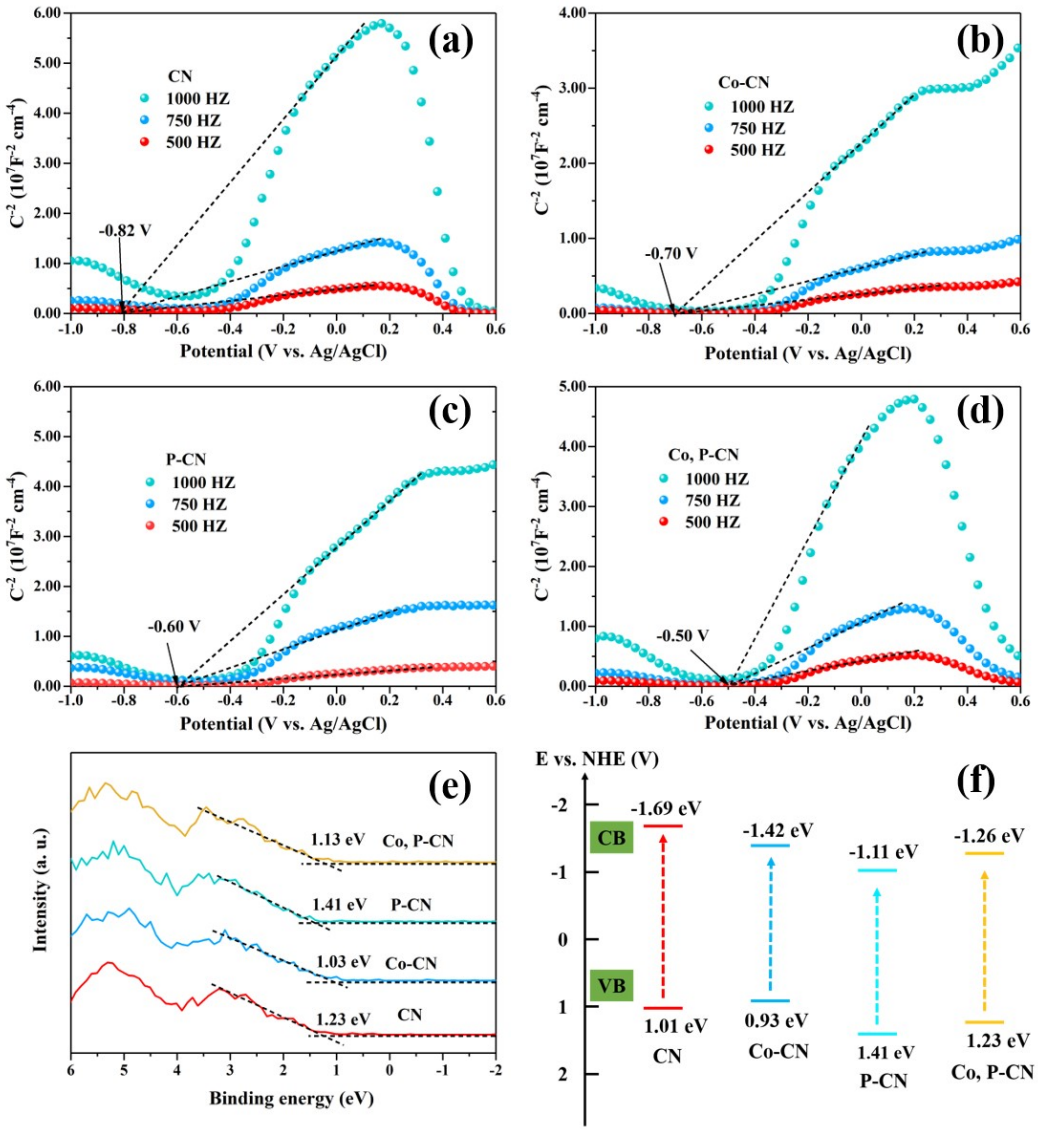

Fig. S8 Mott-Schottky plots (a-d) and (e) VB-XPS, and (f) energy band structure for CN, P-CN, Co-CN, and Co, P-CN samples.

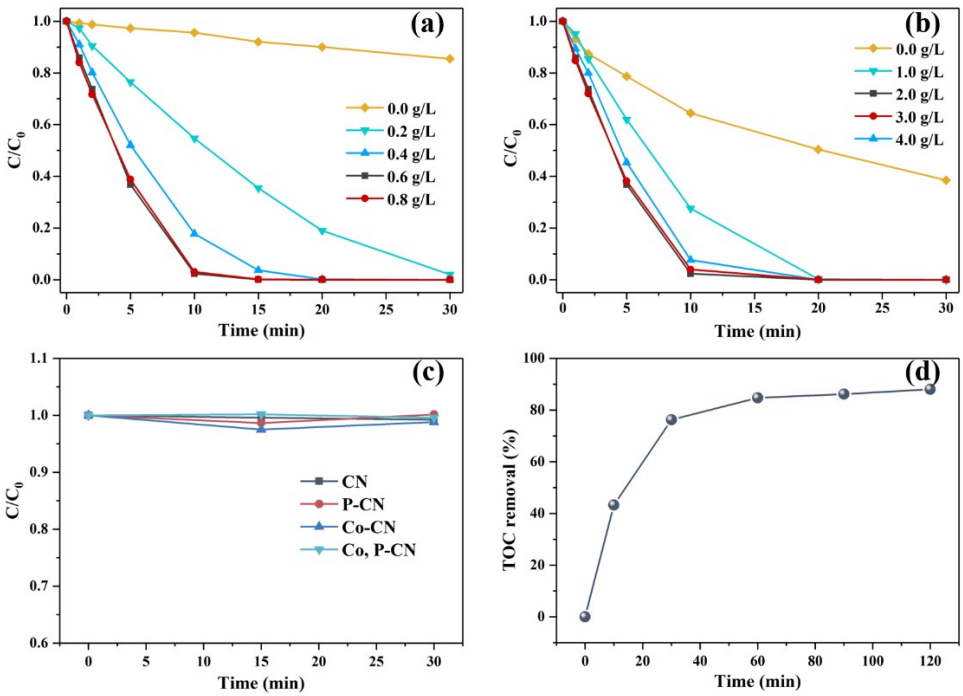

Fig. S9 Operation parameters exploration of (a) catalyst dosage and (b) PDS concentration on BPA photodegradation. (c) The adsorption performance of these samples for BPA under dark condition. (d) The mineralization of BPA over Co, P-CN/PDS/light system (Reaction conditions: $[BPA]_0$=20 mg L^{-1}, [catalyst]=0.6 g L^{-1}, [PDS]=2.0 g L^{-1}).

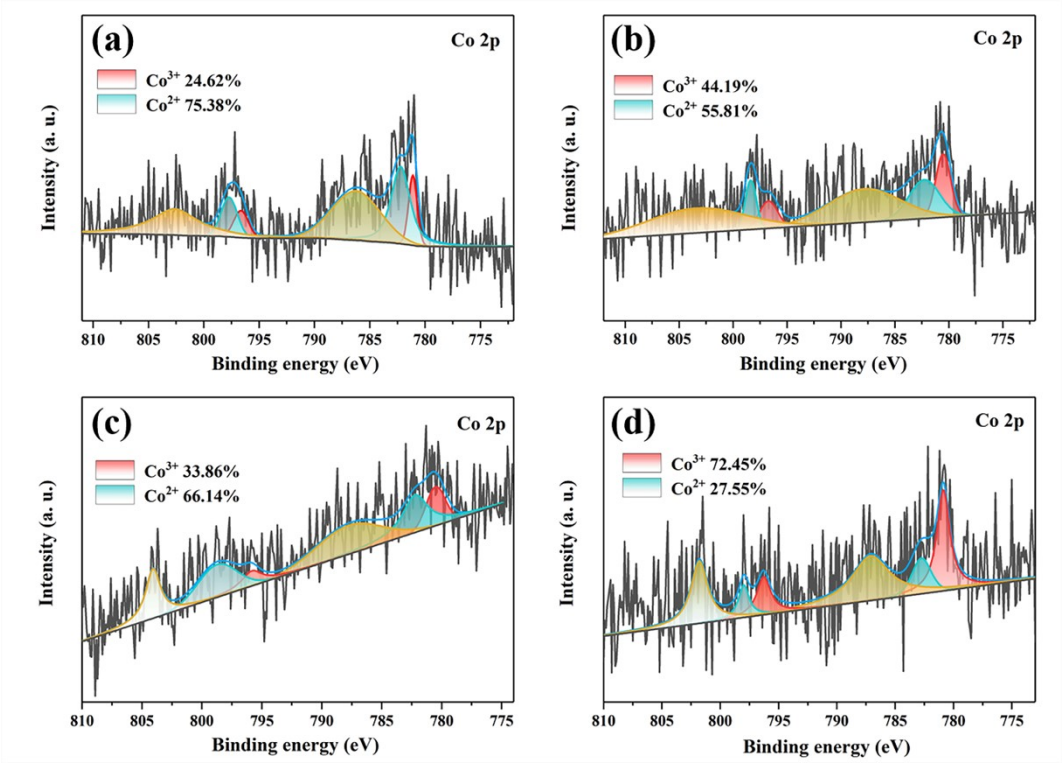

Fig. S10 High-resolution Co 2p XPS spectrum of fresh sample (a), after the 1st cycle sample (b), after the 5th cycle sample (c), and after the 3rd cycle sample (d).

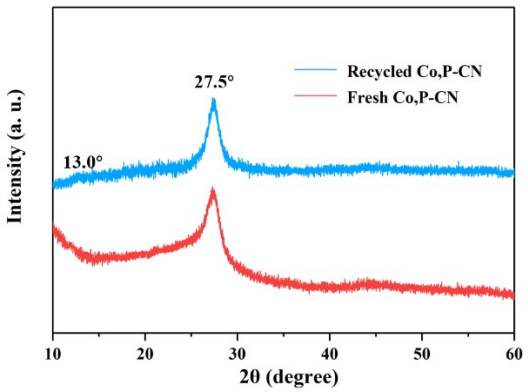

Fig. S11 XRD patterns of recycled and fresh Co, P-CN.

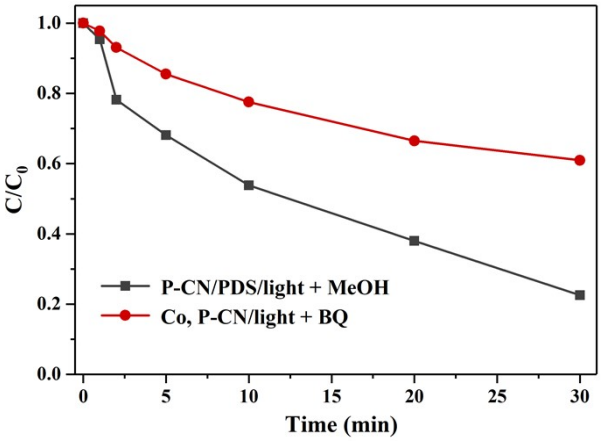

Fig. S12 Degradation of BPA by P-CN/PDS/light system and Co, P-CN/light system with addition of MeOH and BQ radical scavengers, respectively.

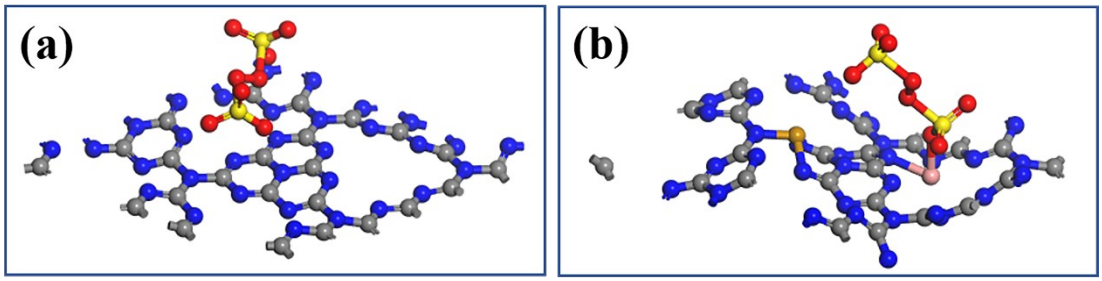

Fig. S13 Adsorption configurations of PDS molecule on pristine g-C_3N_4 (a) and the structure with cobalt doped at site 1 (b). The blue, gray, orange, pink, yellow and red spheres represent C, N, P, Co, S and O atoms, respectively.

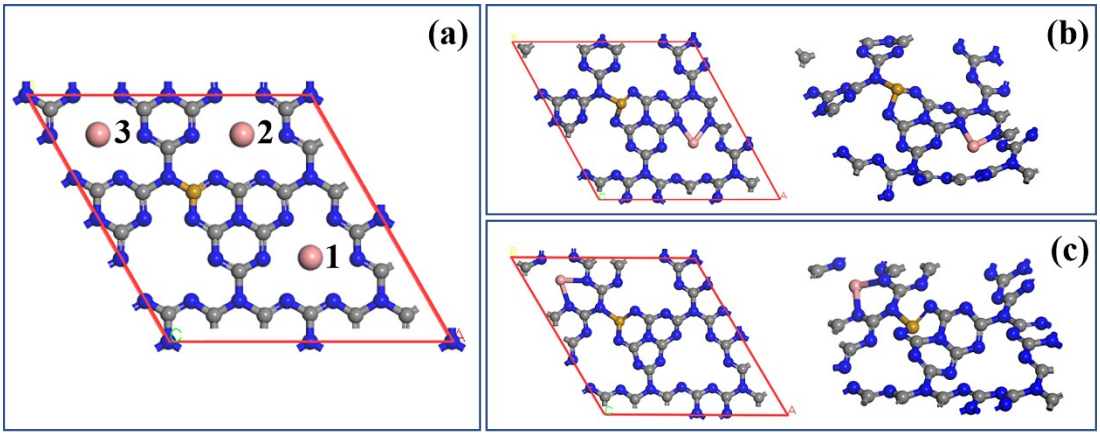

Fig. S14 Three possible doping sites of cobalt on P-CN (a). Top and side views of the optimized structures with cobalt doped at site 1(b) and site 3 (c).

Table S1. BET surface areas, pore volumes, and pore size of as-prepared samples.

Catalysts	S (m^2/g)	V (cm^3/g)	Pore size (nm)
CN	98.97	0.579	13.23
P-CN	124.19	0.853	17.56
Co-CN	128.53	1.026	19.60
Co, P-CN	165.64	1.871	28.14

Table S2. Atom concentration for C, N, P, and Co elements derived from the XPS spectra.

Samples	C (at %)	N (at %)	P (at %)	Co (at %)	C/N atom ratio
CN	45.88	54.12	-	-	0.85
P-CN	42.72	55.99	1.29	-	0.76
Co-CN	44.20	55.49	-	0.31	0.80
Co, P-CN	42.95	55.63	1.01	0.45	0.77

Table S3. The contents (%) of different valence bonds of C and N determined from deconvoluted XPS spectra.

Samples	C 1s		N 1s			
	C-C/C=C	N-C=N	C-N=C	$N-(C)_3$	C-N-H	Charging effect
CN	7.59	92.41	54.60	28.50	5.98	10.92
P-CN	12.62	87.38	53.31	29.54	6.11	11.04
Co-CN	7.41	92.59	60.72	22.27	5.52	11.49
Co, P-CN	16.91	83.09	53.17	29.01	8.25	9.57

Table S4. Photocatalytic degradation various pollutants by g-C_3N_4 based materials activated PMS/PDS.

Catalysts (loading, g/L)	Light source	Pollutants (mg/L)	PMS/PDS (g/L)	Removal Efficiency	Cycling test (degradation rate (%)/K (min^{-1}))	Ref
G-C_3N_4 nanosheets (0.5)	150 W Xe (>400 nm)	BPA (5)	PDS (1.2)	100% (90 min)	--	7
Co_3O_4/g-C_3N_4/$Bi_2O_2CO_3$ (1.0)	1000 W Xe	IOH (20)	PDS (3.0)	94% (60 min)	4th run (80%)	8
N-deficient g-C_3N_4 (0.4)	30 W LED (410-760 nm)	TC (10)	PDS (2.0)	85% (60 min)	3rd run (79%)	9
G-C_3N_4 (0.05)	300 W Xe	SMX (10)	PDS (0.5)	98.4% (60 min)	3rd run (94%)	10
g-C_3N_4/Fe_2O_3 (0.5)	LED	BPA (114)	PDS (2.7)	92.2% (60 min)	5th run (83.2%)	11
5% g-C_3N_4-TiO_2 (0.5)	300 W Xe (>400 nm)	AAP (5)	PDS (2.0)	99.3% (30 min)	5th run (94.3%)	12
O-C_3N_4 (0.5)	300 W Xe	BPA (20)	PDS	100% (30 min)	3rd run (~97%)	13
Pd/g-C_3N_4 (1.0)	500 W Xe (>420 nm)	BZF (3)	PMS (0.4)	86% (180 min)	3rd run (~55%)	14
ZIF-NC/g-C_3N_4	300 W Xe (>400 nm)	BPA (20)	PMS (0.4)	97% (60 min)	5th run (85%)	15
Co_3O_4-g-C_3N_4 (0.5)	300 W electric power and 50 W luminous power Xe lamp (>420 nm)	DCF (10)	PMS (0.31)	100% (30 min)	--	16
Ag/AgCl@ZIF-8/g-C_3N_4 (1.0)	150 W Xe (>420 nm)	LVFX (10)	PMS (1.23)	87.3% (60 min)	4th run (79%)	17
Ag/mpg-C_3N_4 (0.1)	300 W Xe (>400 nm)	BPA (20)	PMS (0.62)	100% (60 min)	4th run (76%)	18
C_3N_4@$MnFe_2O_4$-G (1.0)	300 W Xe (>400 nm)	MNZ (20)	PDS (2.7)	94.5% (90 min)	5th run (~81%)	19
G-C_3N_4/Fe (III) (1.88)	350 W Xe	Phenol (10)	PDS	33% (90 min)	--	20
Fe^0/C_3N_4 (0.4)	350 W Xe (>400 nm)	RhB (20)	PDS (0.81)	100% (40 min)	3rd run (~80%)	21
CNS (0.3)	150 W lamp	RhB (50)	PMS (0.3)	~100% (120 min)	5th run (~90%)	22
G-C_3N_4-550 (0.4)	500 W Xe (>420 nm)	AO7 (20)	PMS (0.2)	96.3% (30 min)	5th run (~80%)	23
G-C_3N_4@$CoFe_2O_4$/Fe_2O_3 (0.33)	500 W Xe (>400 nm)	TC (30)	PDS (0.67)	100% (80 min)	5th run (99%)	24
Ti_3C_2/g-C_3N_4 (0.25)	300 W Xe	DCF (10)	PMS (0.25)	100% (30 min)	5th run (98%)	25
CeO_2/g-C_3N_4 (1.0)	150 W (>420 nm)	NOR (10)	PDS (1.35)	88.6% (60 min)	3rd run (~88%)	26
D35-TiO_2/g-C_3N_4 (0.5)	300 W Xe (>400 nm)	BPA (10)	PDS (0.54)	100% (15 min)	5th run (93%)	27
Co, P-CN (0.6)	300 W Xe	BPA (20)	PDS (2.0)	99.98% (10 min)	5th run (100%, 0.159 min^{-1})	**This work**

Table S5. Scavengers used, active species quenched and *k* value of BPA degradation in Co, P-

CN/PDS/light system.

Scavengers	Active species	k (min^{-1})
No scavengers	/	0.375
TBA	•OH	0.128
MeOH	$SO_4^{\bullet-}$ and •OH	0.027
$K_2Cr_2O_7$	e^-	0.039
TEOA	h^+	0.038
EDTA-2Na	h^+	0.020
BQ	$O_2^{\bullet-}$	0.009
FFA	$^1O_2$	0.005

Table S6. Active species in different systems and theirs related generation equations.

Systems	Active species	Equations
PDS/light	/	/
Co, P-CN/PDS/dark	$O_2^{\bullet-}$, $^1O_2$, $SO_4^{\bullet-}$ and •OH	$\equiv Co^{2+}+3S_2O_8^{2-}+2H_2O \longrightarrow O_2^{\bullet-}+2SO_4^{\bullet-}+4SO_4^{2-}+4H^++\equiv Co^{3+}$ (S3)
		$O_2^{\bullet-}+S_2O_8^{2-} \longrightarrow {}^1O_2+SO_4^{\bullet-}+SO_4^{2-}$ (S4)
		$2O_2^{\bullet-}+2H_2O \longrightarrow {}^1O_2+H_2O_2+2OH^-$ (S5)
		$SO_4^{\bullet-}+H_2O \longrightarrow \bullet OH+ SO_4^{2-}+H^+$ (S6)
		$H_2O_2 \longrightarrow 2\bullet OH$ (S7)
		$O_2^{\bullet-}/{}^1O_2/SO_4^{\bullet-}/\bullet OH+BPA \longrightarrow \ldots \longrightarrow$ Small molecules (S8)
Co, P-CN/light	$O_2^{\bullet-}$, $^1O_2$, •OH and h^+	Co, P-CN+hν $\longrightarrow$ e^-+h^+ (S9)
		$O_2+e^- \longrightarrow O_2^{\bullet-}$ (S10)
		$O_2^{\bullet-}+h^+ \longrightarrow {}^1O_2$ (S11)
		Eqs. (S5) and (S7)
		$O_2^{\bullet-}/{}^1O_2/\bullet OH/h^++BPA \longrightarrow \ldots \longrightarrow$ Small molecules (S12)
Co, P-CN/PDS/light	$O_2^{\bullet-}$, $^1O_2$, $SO_4^{\bullet-}$, •OH and h^+	Eqs. (S9) and (S10)
		$S_2O_8^{2-}+e^- \longrightarrow [S_2O_8^{2-}]$ (S13)
		$[S_2O_8^{2-}]+O_2 \longrightarrow S_2O_8^{2-}+ O_2^{\bullet-}$ (S14)
		Eqs. (S4), (S5) and (S11)
		$S_2O_8^{2-}+e^- \longrightarrow SO_4^{\bullet-}+SO_4^{2-}$ (S15)
		Eq. (S3)
		$\equiv Co^{3+}+ e^- \longrightarrow \equiv Co^{2+}$ (S16)
		Eqs. (S6) and (S7)
		$O_2^{\bullet-}/{}^1O_2/SO_4^{\bullet-}/\bullet OH/h^++BPA \longrightarrow \ldots \longrightarrow$ Small molecules (S17)

Table S7. The adsorption energy (E_{ads}) and O-O bond length (l_{O-O}) of several different adsorption

configurations of PDS molecule on pristine g-C_3N_4 and Co, P-CN.

Adsorption configurations	E_{ads} (eV)	Q (e)	l_{O-O} (Å)
Free PDS	--	--	1.319
g-C_3N_4	-0.179	0.787	1.307
Type 1	-1.006	0.726	1.503
Type 2	-0.160	0.500	1.517
Type 3	-0.447	1.429	1.500
Type 4	-1.285	1.482	1.515
Type 5	-0.600	0.865	1.325
Type 6	-0.251	1.011	1.321
Type 7	-0.209	1.128	1.312

References

1 Y. L. Wu, F. L. Wang, X. Y. Jin, X. S. Zheng, Y. F. Wang, D. D. Wei, Q. X. Zhang, Y. P. Feng, Z. J. Xie, P. Chen, H. J. Liu and G. G. Liu, *Water Res*., 2020, **172**, 115492.
2 X. G. Duan, C. Su, L. Zhou, H. Q. Sun, A. Suvorovac, T. Odedairo, Z. H. Zhu, Z. P. Shao and S. B. Wang, *Appl. Catal. B: Environ*., 2016, **194**, 7-15.
3 P. E. Blöchl, *Phys. Rev. B*, 1994, **50**, 17953-17979.
4 G. Kresse and J. Furthmuller, *Phys. Rev. B*, 1996, **54**, 11169-11186.
5 J. P. Perdew, K. Burke and M. Ernzerhof, *Phys. Rev. Lett*., 1996, **77**, 3865-3868.
6 R. F. W. Bader, *Clarendon Press*, 1994.
7 B. C. Liu, M. Qiao, Y. B. Wang, L. J. Wang, Y. Gong, T. Guo and X. Zhao, *Chemosphere*, 2017, **189**, 115-122.
8 W. M. Xiang, Q. Y. Ji, C. M. Xu, Y. Guo, Y. Z. Liu, D. Y. Sun, W. W. Zhou, Z. Xu, C. D. Qi, S. G. Yang, S. Y. Li, C. Sun and H. He, *Appl. Catal. B: Environ*., 2021, **285**, 119847.
9 H. R. Sun, F. Guo, J. J. Pan, W. Huang, K. Wang and W. L. Shi, *Chem. Eng. J*., 2021, **406**, 126844.
10 Y. L. Song, L. Huang, X. J. Zhang, H. Z. Zhang, L. Wang, H. Zhang and Y. L. Liu, *J. Hazard. Mater*., 2020, **393**, 122379.
11 S. D. Yan, Y. Shi, Y. F. Tao and H. Zhang, *Chem. Eng. J*., 2019, **359**, 933-943.
12 X. Y. Du, X. Bai, L. Xu, L. Yang and P. K. Jin, *Chem. Eng. J*., 2020, **384**, 123245.
13 Q. W. Tang, X. Q. An, J. Zhou, H. C. Lan, H. J. Liu and J. H. Qu, *J. Colloid Interf. Sci.*, 2020, **579**, 455-462.
14 Z. Yin, M. G. Han, Z. Hu, L. Feng, Y. Z. Liu, Z. W. Du and L. Q. Zhang, *Chem. Eng. J*., 2020, **390**, 124532.
15 Y. Gong, X. Zhao, H. Zhang, B. Yang, K. Xiao, T. Guo, J. J. Zhang, H. X. Shao, Y. B. Wang and G. Yu, *Appl. Catal. B: Environ*., 2018, **233**, 35-45.
16 H. X. Shao, X. Zhao, Y. B. Wang, R. Mao, Y. Wang, M. Qiao, S. Zhao and Y. F. Zhu, *Appl. Catal. B: Environ.*, 2017, **218**, 810-818.
17 J. B. Zhou, W. Liu and W. Q. Cai, *Sci. Total Environ*., 2019, 696, 133962.
18 Y. B. Wang, X. Zhao, D. Cao, Y. Wang and Y. F. Zhu, *Appl. Catal. B: Environ.*, 2017, **211**, 79-88.
19 X. Y. Wang, A. Q. Wang and J. Ma, *J. Hazard. Mater*., 2017, **336**, 81-92.
20 J. Y. Hu, K. Tian and H. Jiang, *Chemosphere*, 2016, **148**, 34-40.
21 H. Heidarpour, M. Padervand, M. Soltanieh and M. Vossoughi, *Chem. Eng. Res. Des.*, 2020, **153**, 709-720.
22 K. Y. A. Lin and Z. Y. Zhang, *Chem. Eng. J.*, 2017, **313**, 1320-1327.
23 X. W. Jiang, J. Li, J. Fang, L. Gao, W. X. Cai, X. X. Li, A. H. Xu and X. C. Ruan, *J. Photoch. Photobio. A*, 2017, **336**, 54-62.
24 S. W. Lv, J. M. Liu, N. Zhao, C. Y. Li, F. E. Yang, Z. H. Wang and S. Wang, *Sep. Purif. Technol*., 2020, **253**, 117413.
25 J. He, J. L. Yang, F. X. Jiang, P. Liu and M. S. Zhu, *Chemosphere*, 2020, **258**, 127339.
26 W. Liu, J. B. Zhou and J. Yao, *Ecotoxicol. Environ. Saf*., 2020, **190**, 110062.
27 L. Yang, X. Bai, J. Shi, X. Y. Du, L. Xu and P. K. Jin, *Appl. Catal. B: Environ*., 2019, **256**, 117759.